ARTICLE

Multi-colored hollow carbon-containing titania nanoshells for anti-counterfeiting applications

Received 00th January 20xx,
Accepted 00th January 20xx

DOI: 10.1039/x0xx00000x

Xiaxi Yao,*[,a,b] Yaocai Bai,[b] Yoon Jae Lee,[b] Zhimin Qi,[b] Xiaoheng Liu,[c] Yadong Yin*[,b]

While titania and carbon are conventionally perceived as white and black materials, here we show that their combination in the form of composite hollow nanoshells can display striking colors with considerably high contrast through resonant Mie scattering. Our unique design utilizes the hollow nanostructures to produce the color by minimizing the random multiple scattering and the incorporated carbon species to act as an internal black background to suppress the multiple scattering and enhance the color contrast. Synthesized through a simple sol-gel process followed by high-temperature carbonization, these hollow carbon-containing titania (C-TiO_2) nanoshells can exhibit variable bright colors from purple to blue and green by controlling their diameter. They can be conveniently used as alternative pigments in many color-related applications, with the advantages of high chemical and optical stability and low toxicity that are associated with titania and carbon materials and the structural coloration mechanism. In addition, as the visible Mie scattering responds rapidly and reversibly to the changes in the surrounding medium, these nanoshells may also serve as active color components for many applications that require dynamic color switching, such as signage and displays, colorimetric sensors and detectors, and anti-counterfeiting devices.

Introduction

Dyes and pigments are typical sources of color. They selectively absorb incident light of specific frequencies and reflect the remainder to the observer to produce a color. While widely used, they often have limitations in terms of chemical stability and toxicity. Structural coloration is pursued as an alternative mechanism that can create color through constructive interference of light with microscopic structures. Unlike dyes or pigments, structural color can be made much more resistant to fading. Well-known examples include photonic crystals that can exhibit brilliant colors,[1-4] which arise from the coherent Bragg diffraction of light on periodically arranged dielectric materials and can be tuned by changing the periodicity and viewing angle.[5] However, complicated processes are often involved in the creation of the required structural periodicity, significantly limiting their practical applications, especially on large scales. Furthermore, the strong angular dependence, an intrinsic property of Bragg diffraction, is often undesirable for many conventional coloring applications. Scattering is another optical process involving light and matter interaction. A typical type is Rayleigh scattering, which is caused by the scattering of the incident light by particles with dimensions much smaller than its wavelength. This phenomenon is responsible for the blue color of the sky on a sunny day because the blue light with shorter wavelengths is more strongly scattered than the red light. Scattering by particles with sizes comparable to or larger than the light wavelength can be accurately analyzed by the Mie theory.[6] It was recently discovered that hollow nanostructures might significantly enhance the transport mean free path of the incident light, thereby inhibiting the multiple scattering and making the color from Mie resonance visible to the naked eye.[7,8] For example, green was produced in submicron magnetite (Fe_3O_4) hollow nanoshells,[9] and multiple colors from blue to green, yellow, and violet were observed from hollow SiO_2 nanoshells of varying sizes against a black background.[7] However, the need for an extra black background to minimize the strong forward scattering puts a substantial limitation on the practical applications of these new structural-color materials that are based on visible Mie scattering.

In this work, we report the design and synthesis of chemically stable and nontoxic hollow carbon-containing titania (C-TiO2) nanoshells that can display bright colors without the need for extra black background. More specifically, TiO_2 shells were produced through a sol-gel process using SiO_2 colloids as hard templates,[10-15] with an internal black background being created through carbonization of the embedded capping ligands. The visible color due to the Mie scattering of the shells is angle independent, and it can be controlled from purple to blue and green by tuning the shell diameter. Compared with previous SiO_2-based systems, the high refractive index of anatase TiO_2 enabled much brighter visible color that can be easily observed by the naked eye. Unlike photonic crystals, the structural color due to visible Mie scattering does not require precise long-

[a] School of Chemistry and Materials Engineering, Changshu Institute of Technology, Changshu 215500, China. Email: xiaxiyao@cslg.edu.cn
[b] Department of Chemistry, University of California, Riverside, California 92521, United States. Email: yadong.yin@ucr.edu
[c] Key Laboratory for Soft Chemistry and Functional Materials of Ministry Education, Nanjing University of Science and Technology, Nanjing 210094, China.

† Electronic Supplementary Information (ESI) available: Digital photograph and TEM image. See DOI: 10.1039/x0xx00000x

range order of the building blocks so the hollow shells can be conveniently deposited onto solid substrates over a large area directly from their colloidal form. As an example, we demonstrate here the spray deposition of the hollow shells into a pattern, which shows a fully reversible color shift in response to solvent exposure as driven by the change of the relative refractive index of the shell to the surrounding medium. The solvent-responsive color shift property allows us to design further a thin film containing a hidden pattern of hydrophobic and hydrophilic areas, which is not recognizable until exposure to water. As TiO_2 has been widely used commercially in areas such as cosmetics, paint, and paper production with their merits of high chemical stability and low toxicity, the added advantages of easy processibility, tunable color, and internal black background will make the C-TiO_2 hollow shells promising alternative pigments for wide potential applications in areas ranging from color coating to anti-counterfeiting devices and colorimetric sensors.

Experimental Section

Synthesis of hollow C-TiO_2 nanoshells

SiO_2 preparation: Colloidal silica templates were synthesized by a modified Stöber method.[16] In a typical process for the synthesis of SiO_2 with 200 nm diameter, tetraethyl orthosilicate (TEOS, 99%, 0.86 mL) was mixed with ethanol (23 mL), deionized water (4.3 mL) and an aqueous solution of ammonia (26%, 0.65 mL). After magnetic stirring for 4 h, the silica particles were collected by centrifugation, washed three times with ethanol, and then re-dispersed in 5 mL of ethanol. The SiO_2 with different sizes can be fabricated with a similar method by optimizing the amount of water and ammonia.

TiO_2 coating: The dispersed 5 mL of SiO_2 suspension was added to the mixture of ethanol (15 mL), acetonitrile (ACN, 7 mL), and hydroxypropyl cellulose (HPC, 0.05 g). After magnetic stirring for 15 min, 0.2 mL of $NH_3 \cdot H_2O$ was subsequently added. Finally, the mixture of titanium n-butoxide (TBOT, 1 mL), ethanol (3 mL) and ACN (1 mL) was injected quickly into the above system. The precipitate was separated by centrifugation after stirring for 2 h and washed 3 times with ethanol and 2 times with water. Then, the as-obtained SiO_2@TiO_2 sample was re-dispersed in 20 mL of de-ionized water.

Partial etching and HCl treatment: In order to maintain the structural integrity and get well-crystallized TiO_2, it is necessary to create a space between SiO_2 core and TiO_2 shell for the growth of TiO_2 nanocrystals in the calcination process. The partial etching is an efficient way to remove the portions of SiO_2 in contact with the TiO_2 surface. The above 20 mL of SiO_2@TiO_2 suspension was partially etched with NaOH (1 mL, 2.5 M) for 20 min at room temperature. The partially etched SiO_2@TiO_2 particles were isolated by centrifugation, washed 3 times with water, re-dispersed in 10 mL of water, mixed with 2 mL 0.5 M HCl aqueous solution, and stirred for 30 min. The final products were collected by centrifugation, washed with water and ethanol, and dried for 6 h under vacuum at room temperature. The purpose of the HCl treatment is to convert sodium titanates to protonated titanates.[11]

Calcination and SiO_2 full etching: The SiO_2@TiO_2 after HCl treatment was calcined at 700 °C for 3 h at a heating rate of 2.5 °C/min under an anaerobic atmosphere. Then, the calcined samples were dispersed in 26 mL of deionized water and heated to 90 °C. An aqueous NaOH solution (2.5 M, 4 mL) was injected into the above suspension. After etching for 4h, the hollow C-TiO_2 particles were collected by centrifugation, washed several times with water and ethanol, and dried for 6 h under vacuum at room temperature. The final samples were named as D(T)@C-TiO_2. D and T represented the inner diameter and shell thickness (nm) of the hollow nanoshells, respectively. For comparison, irregularly-shaped solid TiO_2 particles were synthesized using a method similar to that of the TiO_2 hollow nanoshells but in the absence of colloidal SiO_2.

Hydrophobic treatment of hollow C-TiO_2 nanoshells: 100 mg of hollow C-TiO_2 nanoshells were dispersed in 16 ml of 1,2-Dichlorobenzene and 0.3 ml of Trimethoxy(octadecyl)silane and then refluxed at 120 °C for 3 h. The sample was collected by centrifugation and washed several times with isopropanol and ethanol.

Hydrophilic treatment of the sprayed pattern: The sprayed pattern with a mask was treated by plasma (Plasma cleaner, Harrick Plasma). The plasma cleaned area would be hydrophilic.

Characterization

The morphology of the samples was observed by transmission electron microscopy (TEM, FEI Tecnai T12, 120 kV) equipped with an energy-dispersive X-ray spectroscopy (EDS). The phase structure was determined by powder X-ray diffractometer using Cu k_α radiation (Bruker D8 Advance). The reflectance spectra were measured using a probe type Ocean Optics USB4000-UV-vis spectrometer in reflection mode with an integration time of 20 ms. Raman spectra were conducted on a Dilor XY spectrometer excited by a laser at 532 nm.

Results and discussion

Well-defined hollow TiO_2 shells were synthesized by coating TiO_2 on colloidal SiO_2 templates, partially etching with NaOH, and treating in HCl solution, followed by calcination under anaerobic atmosphere and a full etching process (Fig. 1). Fig. 2 shows the corresponding TEM images of the SiO_2@TiO_2 core-shell particles at different synthesis stages. In the case of 200-nm SiO_2 colloidal templates (Fig. 2a), amorphous TiO_2 can be uniformly coated on the surface of SiO_2 by hydrolyzing titanium n-butoxide (TBOT) precursor with hydroxypropyl cellulose (HPC) as the surfactant (Fig. 2b). An obvious gap between the SiO_2 core and the TiO_2 shell was formed after partial etching by NaOH and then neutralization by HCl solution (Fig. 2c). Then, the TiO_2 shell crystallized and shrank to the SiO_2 surface after calcination at a high temperature (Fig. 2d). The small gap created by partial etching was favorable for maintaining the shell integrity during the heating process. Without such a gap, direct calcination of the SiO_2@TiO_2 core-shell particles could

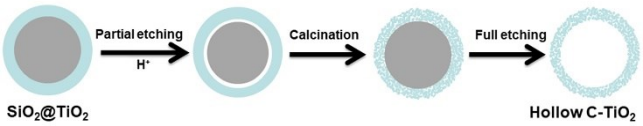

Fig. 1 Schematic illustration of the synthesis of hollow C-TiO_2 nanoshells.

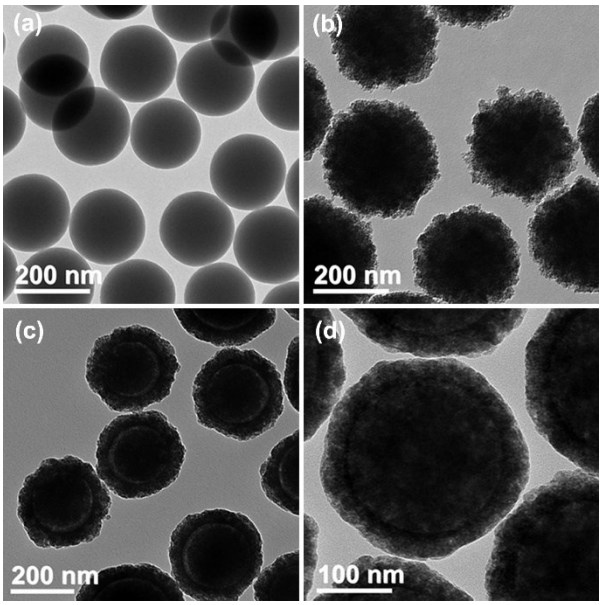

Fig. 2 TEM images of samples at different stages of synthesizing SiO_2@TiO_2 spheres, in order: (a) colloidal SiO_2 templates, (b) after TiO_2 coating, (c) after partial etching with NaOH and then HCl treatment, (d) after calcination in Ar.

induce significant growth of the TiO_2 grains and eventually break the shells.[17] The purpose of the HCl treatment was to replace sodium ions by cation exchange and avoid the formation of sodium titanate phase, which could also crystallize into large domains upon calcination and destroy the shell integrity. Further, heating under an anaerobic atmosphere led to carbonization of the TBOT precursor and HPC surfactant, generating carbon species in the shell as evidenced by the dark gray color of the samples.[18,19] Two controllable experiments were conducted to confirm our understanding of the carbon formation: (1) Pure TiO_2 nanoparticles were synthesized using a similar method to the TiO_2 coating but in the absence of colloidal SiO_2 and HPC surfactant, followed by calcination at 700 ^oC for 3h under an anaerobic atmosphere; (2) HPC powder was directly calcined at 700 ^oC for 3h under an anaerobic atmosphere. After calcination, both samples appeared black, suggesting the formation of carbon species (Fig. S1).

After removing the SiO_2 core by full etching with NaOH solution, the integrity of the hollow shells can be well maintained without any breakage. The final C-TiO_2 hollow nanoshells contain anatase TiO_2 with no observable sodium titanate according to the XRD pattern (Fig. S2). No obvious diffraction peaks were found for crystallized carbon, indicating the formation of amorphous carbon. Ti, O, C, and Si elements were uniformly distributed on the shell surface without any aggregation according to the EDS elemental mapping (Fig. S3). The carbon resulted from the carbonation of HPC and organic species in TBOT during the calcination process, which accounted for about 12.6% molar ratio in the shell. Only a small amount of Si (2.6%) remained in the shell after etching in NaOH solution.

A series of hollow C-TiO_2 nanoshells were synthesized with different diameters by simply tuning the size of the SiO_2 templates. The hollow particle size and the shell thickness were determined by transmission electron microscopy (TEM) (Fig. 3a-d). The final samples were named in the form of D(T)@C-TiO_2, with D and T representing the inner diameter and shell thickness (nm) of the hollow nanoshells, respectively. Almost all of the hollow samples had a similar shell thickness around 18-22 nm, which represented the minimum thickness necessary to maintain the shell. Interestingly, the hollow particles with different diameters displayed unique and uniform colors of gray, purple, blue, and green after full etching and drying (Fig. 3e-h). Although disordered, the resulting powders displayed bright and angle-independent colors, which were quite

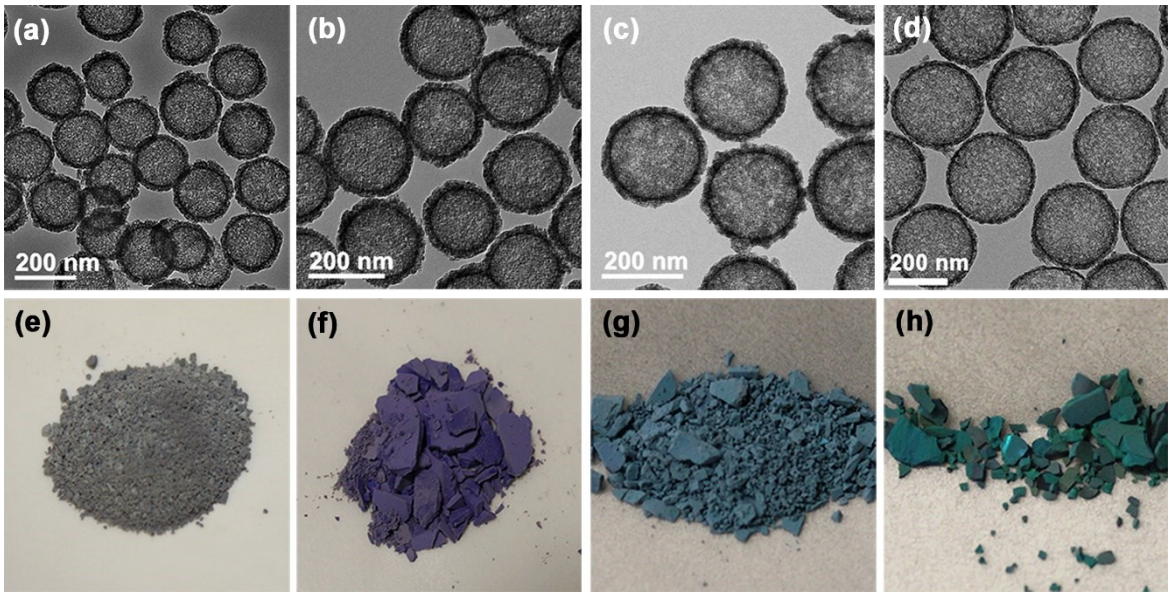

Fig. 3 TEM images and the corresponding digital photographs of hollow C-TiO_2 nanoshells with different diameter and shell thickness: (a, e) inner diameter: 150 nm, shell thickness: 20 nm (150(20)@C-TiO_2); (b, f) inner diameter: 180 nm, shell thickness: 22 nm (180(22)@C-TiO_2); (c, g) inner diameter: 220 nm, shell thickness: 22 nm (220(22)@C-TiO_2); (d, h) inner diameter: 268 nm, shell thickness: 18.5 nm (268(18.5)@C-TiO_2).

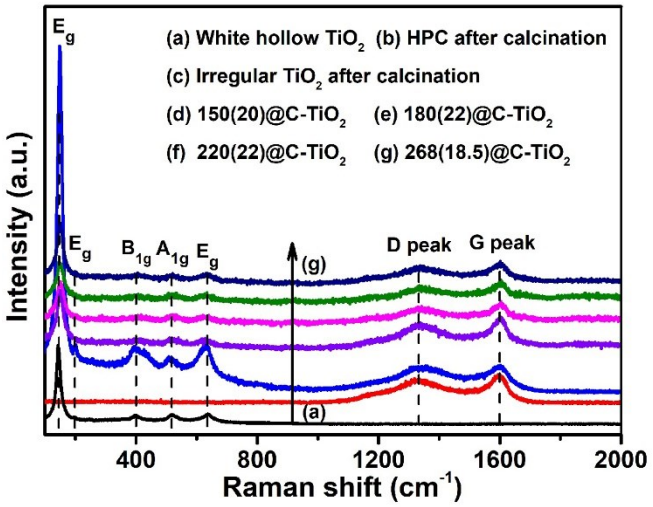

Fig. 4 Raman spectra of the as-synthesized hollow C-TiO_2 nanoshells and the reference samples.

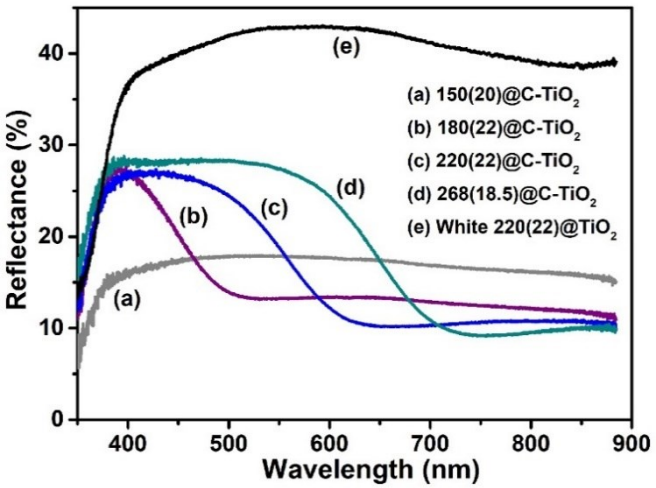

Fig. 5 Reflectance spectra of hollow C-TiO_2 nanoshells with different inner diameters.

different from the iridescent colors caused by Bragg diffraction in periodic photonic crystals. The color of the hollow C-TiO_2 nanoshells can maintain the initial brightness even after being stored for over one year, indicating the high stability. For comparison, the irregularly-shaped solid TiO_2 particles were synthesized using a method similar to that of the TiO_2 hollow nanoshells but in the absence of colloidal SiO_2. After calcination under anaerobic atmosphere, the color appeared to be black (Fig. S4). In addition, the bright colors of the purple, blue or green samples disappeared and changed to gray upon destroying the shell structure by grinding in an agate mortar. Since the only difference in the samples before and after grinding was the morphology, one can appreciate the key role of hollow shell structure in determining the appearance of the bright colors.

The hollow structure can significantly increase the transport mean free path of the incident light, allowing light to propagate back and forth inside the shell to escape the powder with reduced multiple scattering and producing constructive interference with the light directly scattered from the nanoshells.[7,8,20] Generally, the forward scattering is considerably stronger than the backscattering.[21] Thomas et al. demonstrated that the visible Mie resonance could be observed by the naked eye when a black background was used to absorb the strong forward scattering.[7] In our case, the hollow C-TiO_2 nanoshells exhibited vivid multi-colors without the need for the extra black background because the C species in the TiO_2 shell resulted from the carbonization of TBOT and HPC could act as the internal dark background. Raman spectra were used to characterize the existence of the carbon species in the hollow TiO_2 shells. Fig. 4 revealed the room-temperature Raman spectra of the as-synthesized samples excited by a laser at 532 nm. For the hollow TiO_2 nanoshells calcined under air (Fig. 4a), there were five vibration peaks at 144, 197, 400, 518 and 637 cm^{-1}, which could be attributed to the Raman-active modes of anatase TiO_2 with the symmetries of E_g, E_g, B_{1g}, A_{1g}, and E_g, respectively.[22-25] The D and G peaks were clearly detected at 1336 and 1602 cm^{-1} for the carbonized product of HPC calcined under the anaerobic atmosphere, and the relative intensity of G peak was slightly higher than that of D peak, indicating the existence of graphitic carbon (Fig. 4b). The Raman spectrum of the irregular TiO_2 particles calcined under anaerobic atmosphere showed the coalescent peaks of anatase TiO_2 and graphitic carbon, and the carbon arose from the carbonization of organic species in TBOT (Fig. 4c). The hollow C-TiO_2 nanoshells with different diameters showed similar Raman spectra, which confirmed the existence of graphitic carbon in the anatase TiO_2 shells (Fig. 4d-g).

Detailed characterization of the optical properties of the powder samples was conducted by measuring the reflectance spectra in a probe type Ocean Optics USB UV-vis spectrometer. As widely known, anatase TiO_2 is a typical metal oxide semiconductor with a band gap of ~3.2 eV. Both scattering and absorption are effective at the wavelength below the absorption edge, while only scattering needs to be considered at a longer wavelength. In this work, we mainly focused on the color observation above 350 nm from visible Mie scattering in hollow nanoshells. As shown in Fig. 5, all the spectra of hollow C-TiO_2 nanoshells displayed a broad peak, and the peak position clearly moved toward longer wavelengths with increasing shell diameters. For the smallest particles, no scattering peak was found in the detectable range (350-900 nm) (Fig. 5a) and therefore this sample exhibited the grayish color. The peaks centered at 397, 453, and 505 nm corresponded to the purple, blue, and green colors of the hollow C-TiO_2 shells with different diameters (Fig. 5b-d), well consistent with the colors observed in the hollow samples in Fig. 3. For comparison, the reflectance spectrum of white hollow TiO_2 shells calcined under air was also analyzed. As depicted in Fig. 5e, it displayed a high reflection in the visible region because the multiple scattering occurred, and the anatase TiO_2 could not absorb visible light due to its large band gap. However, the reflection of hollow C-TiO_2 nanoshells in the visible region was very low except for the resonant peaks because the C species in the shell could absorb the incident light and multiple scattering,[26,27] and only the stronger light from the resonant Mie scattering can escape the powder before being

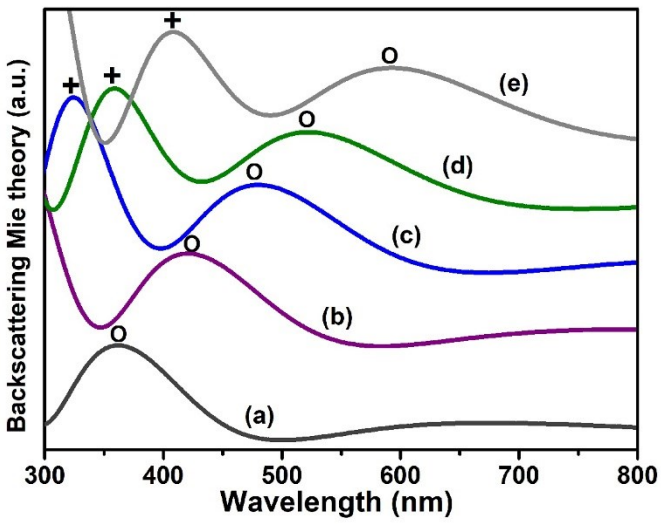

Fig. 6 Simulation of the Mie backscattering for the hollow C-TiO_2 nanoshells with different diameters and shell thicknesses: (a) 150(20)@C-TiO_2; (b) 180(22)@C-TiO_2; (c) 220(22)@C-TiO_2; (d) 268(18.5)@C-TiO_2; (e) 310(20)@C-TiO_2. (Open circles and crosses represent different modes of Mie resonance)

absorbed and can be detected by the spectrometer or observed by the bare eye.

The Mie resonance of hollow C-TiO_2 nanoshells can be predicted by computing the backscattering spectra using the Matlab calculation code provided by Mäetzler.[28,29] In 1908, Gustav Mie first proposed the theory to exactly analyze the scattering from a perfect and homogeneous sphere when the size of the scattering particles is comparable to the wavelength of the incident light.[6,30] In general, Mie scattering is characterized by the following parameters, including scattering efficiency Q_{sca}, absorption efficiency Q_{abs}, extinction efficiency Q_{ext}, backscattering efficiency Q_b, and the asymmetry factor cosθ. All of them can be calculated based on the Mie coefficients a_n and b_n.[9,29,30] For the model of hollow nanoshells, a_n and b_n are computed as:

$$a_n = \frac{\psi_n(y)[\psi_n'(m_2y) - A_n\chi_n'(m_2y)] - m_2\psi_n'(y)[\psi_n(m_2y) - A_n\chi_n(m_2y)]}{\xi_n(y)[\psi_n'(m_2y) - A_n\chi_n'(m_2y)] - m_2\xi_n'(y)[\psi_n(m_2y) - A_n\chi_n(m_2y)]}$$

$$b_n = \frac{m_2\psi_n(y)[\psi_n'(m_2y) - B_n\chi_n'(m_2y)] - \psi_n'(y)[\psi_n(m_2y) - B_n\chi_n(m_2y)]}{m_2\xi_n(y)[\psi_n'(m_2y) - B_n\chi_n'(m_2y)] - \xi_n'(y)[\psi_n(m_2y) - B_n\chi_n(m_2y)]}$$

with

$$A_n = \frac{m_2\psi_n(m_2x)\psi_n'(m_1x) - m_1\psi_n'(m_2x)\psi_n(m_1x)}{m_2\chi_n(m_2x)\psi_n'(m_1x) - m_1\chi_n'(m_2x)\psi_n(m_1x)}$$

$$B_n = \frac{m_2\psi_n(m_1x)\psi_n'(m_2x) - m_1\psi_n(m_2x)\psi_n'(m_1x)}{m_2\chi_n'(m_2x)\psi_n(m_1x) - m_1\chi_n'(m_1x)\chi_n(m_2x)}$$

where m_1 and m_2 are the complex refractive indices of the inner core and outer shell relative to the surrounding medium. $m_1=n_1/n_0$ and $m_2=n_2/n_0$, where n_0, n_1, and n_2 represent the refractive indices of the surrounding medium, inner core, and outer shell, respectively. The size parameters x and y are defined as $x=\pi n_0 d_1/\lambda$ and $y = \pi n_0 d_2/\lambda$, in which d_1 and d_2 are the diameters of the inner core and outer shell, and λ is the wavelength of the incident light in vacuum.[9,30,31] ψ_n, χ_n, ξ_n are the Bessel-Riccatti functions. Subsequently, Q_{sca}, Q_{ext}, Q_b, and cos θ are obtained:

$$Q_{sca} = \frac{2}{y^2}\sum_{n=1}^{N}(2n+1)(|a_n|^2 + |b_n|^2)$$

$$Q_{ext} = \frac{2}{y^2}\sum_{n=1}^{N}(2n+1)\,\mathrm{Re}(a_n + b_n)$$

$$Q_b = \frac{1}{y^2}\left|\sum_{n=1}^{N}(2n+1)(-1)^n(a_n - b_n)\right|^2$$

$$\cos\theta = \frac{4}{y^2 Q_{sca}}\left\{\sum_{n=1}^{N}\frac{n(n+2)}{n+1}\mathrm{Re}(a_n a_{n+1}^* + b_n b_{n+1}^*) + \sum_{n=1}^{N}\frac{2n+1}{n(n+1)}\mathrm{Re}(a_n b_n^*)\right\}$$

$$N = y + 4y^{1/3} + 2$$

$$Q_{ext} = Q_{sca} + Q_{abs}$$

For the hollow C-TiO_2 nanoshells with a thin shell, the complex refractive index of the hollow shell was optimized as n_2=2.45+0.4i. The refractive index of the hollow shell was about 2.45, which is 6% lower than that of bulk anatase TiO_2 (~2.6) because of the shell porosity and the lower refractive index of amorphous carbon (~2.3). The imaginary part (0.4) was the absorption coefficient of the hollow shell due to the existence of carbon species. The refractive index of air as the core was n_1=1.0. Fig. 6 showed the simulation of backscattering based on Mie theory for the hollow C-TiO_2 nanoshells with different inner diameters and shell thicknesses. As the inner diameter increased, the peak position in the visible region shifted to longer wavelength and more resonant Mie scattering peaks appeared in the wavelength range of 300-800 nm, which meant a second resonant peak with a higher frequency moved to the simulated range when the first peak had a large redshift. For the smallest hollow C-TiO_2 nanoshells (150(20)@C-TiO_2), the simulated scattering peak of Mie resonance was located at 362 nm (Fig. 6a), which corresponded to the grayish color because this peak was in the UV region. When the inner diameter increased to 180 nm with a shell thickness of 22 nm, the resonant scattering peak moved to 417 nm (Fig. 6b), which was well consistent with the observed purple color in the sample of 180(22)@C-TiO_2 hollow nanoshells. Two modes of Mie resonance could be directly distinguished in the wavelength of 300-800 nm as the particle size further increased. The peaks at 476 and 521 nm were attributed to the blue and green colors of hollow C-TiO_2 nanoshells because another mode was situated below 400 nm (Fig. 6c, d). Both two modes were found in the visible region in the case of larger hollow particles with 310 nm inner diameter and 20 nm shell thickness (Fig. 6e). The mixed color of these two peaks at 406 nm and

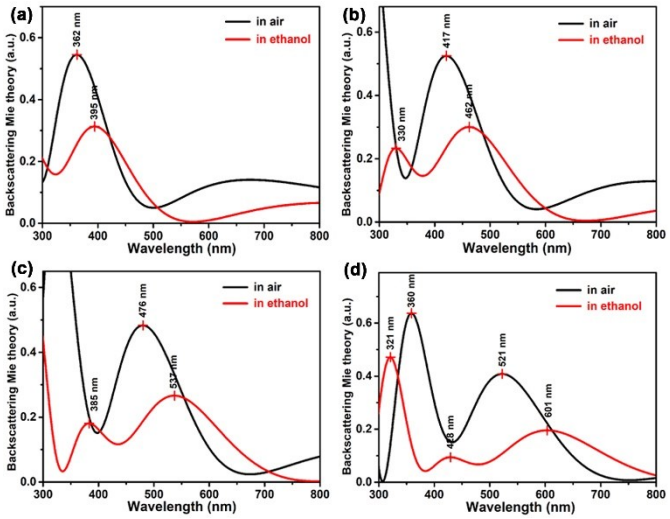

Fig. 7 Simulation of the resonant Mie scattering of hollow C-TiO_2 nanoshells in ethanol: (a) 150(20)@C-TiO_2; (b) 180(22)@C-TiO_2; (c) 220(22)@C-TiO_2; (d) 268(18.5)@C-TiO_2.

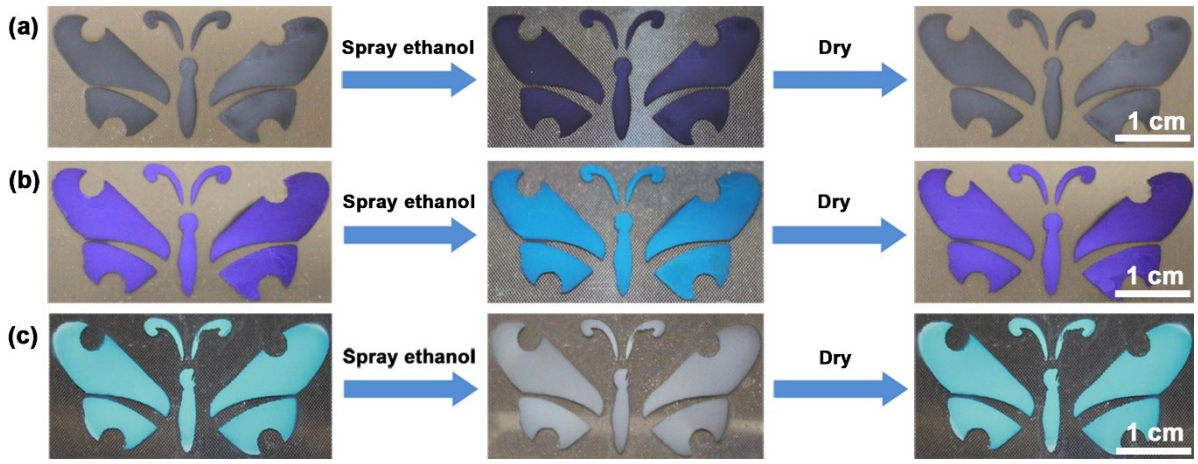

Fig. 8 Color change and restoration of patterns made of various hollow C-TiO_2 nanoshells in response to the addition and evaporation of ethanol. (a) hollow C-TiO_2 nanoshells with inner diameter of 150 nm and shell thickness of 20 nm (150(20)@C-TiO_2); (b) hollow C-TiO_2 nanoshells with inner diameter of 180 nm and shell thickness of 22 nm (180(22)@C-TiO_2); (c) hollow C-TiO_2 nanoshells with inner diameter of 220 nm and shell thickness of 22 nm (2200(22)@C-TiO_2).

591 nm was a grayish tone, and the sample showed an unexpected grayish hue instead of the yellow one (Fig. S5). In brief summary, although the calculations do not precisely resemble the experimental reflectance curves due to the size polydispersity, the simulation of Mie scattering qualitatively clarified the scattering phenomena in hollow C-TiO_2 nanoshells and confirmed the optical observation in Fig. 3.

Based on the Mie theory, the Mie resonance is influenced by the refractive indices of the core and shell materials relative to the surrounding medium. Therefore, the Mie resonance should change when the surrounding medium is altered from air to a solvent such as ethanol (n_0=1.35). The refractive indices of the core (ethanol) and C-TiO_2 shells are n_1=1.35 and n_2=2.45+0.4i. Fig. 7 showed the peak shifts of Mie resonance in hollow C-TiO_2 nanoshells with different surrounding media. For the grayish hollow C-TiO_2 nanoshells (Fig. 7a), the resonant scattering peak had a 33-nm red shift from 362 to 395 nm. The peak shifted from the original 417 nm in air to 462 nm in ethanol in the case of the purple hollow C-TiO_2 nanoshells (Fig. 7b). However, two peaks appeared in the visible region when the blue or green hollow C-TiO_2 nanoshells were exposed to ethanol (Fig. 7c,d). The mixed color of the two peaks at 385 and 537 nm or 428 and 601 nm was almost grayish, and the broader peaks at 537 and 601 nm were also weaker. It is worth noting that the backscattering efficiency decreased slightly after the hollow C-TiO_2 nanoshells were immersed in ethanol due to the reduction of relative refractive indices of C-TiO_2 shell.

To highlight the shift of Mie resonance in air and ethanol, we sprayed the suspensions of hollow C-TiO_2 nanoshells on polystyrene substrates to produce three butterfly patterns. The grayish color of the 150(20)@C-TiO_2 sample rapidly (within 1 s) changed to purple when ethanol was sprayed onto the pattern, and the purple color could completely revert to its original grayish hue upon ethanol evaporation (Fig. 8a). The nanoshells are continuous but they contain many mesopores, which can be observed in the HRTEM image (Fig. S6). Therefore, ethanol can get into the core through the mesoporous structure during the spraying process. The other two

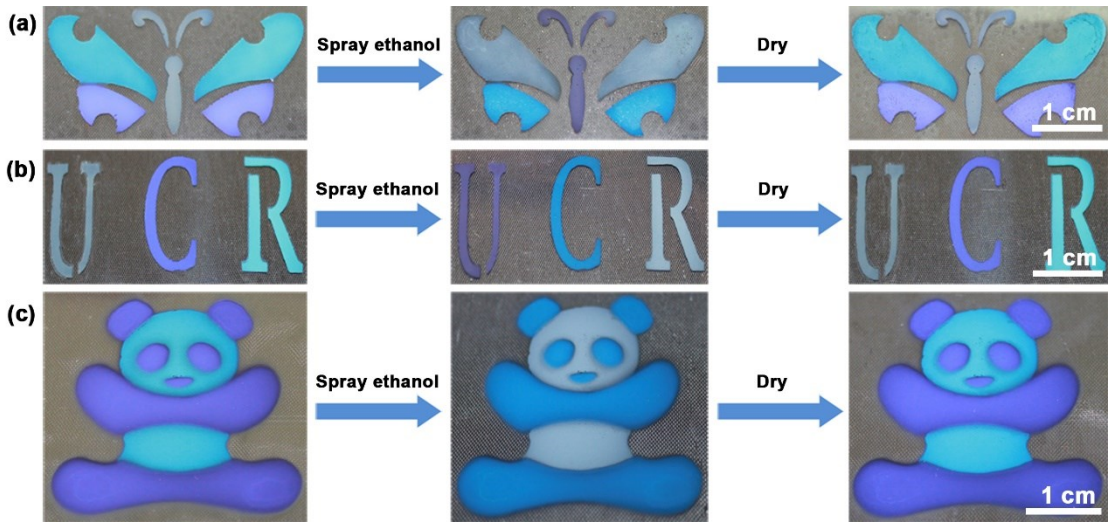

Fig. 9 Color switching of patterns made of multiple hollow C-TiO_2 nanoshells in response to the addition and evaporation of ethanol. The gray sample was hollow C-TiO_2 nanoshells with inner diameter of 150 nm and shell thickness of 20 nm (150(20)@C-TiO_2). The purple sample was hollow C-TiO_2 nanoshells with inner diameter of 180 nm and shell thickness of 22 nm (180(22)@C-TiO_2). The blue sample was hollow C-TiO_2 nanoshells with inner diameter of 220 nm and shell thickness of 22 nm (2200(22)@C-TiO_2).

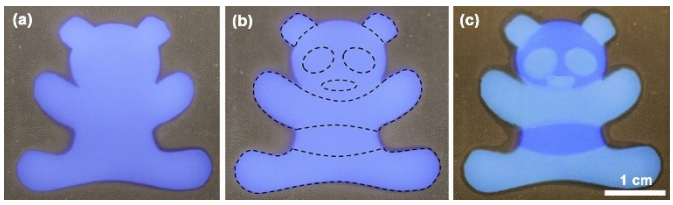

Fig. 10 A hidden pattern that can be revealed by exposing to water: (a) a panda shape by spray-coating hydrophobic hollow C-TiO_2 nanoshells with inner diameter of 180 nm and shell thickness of 22 nm (180(22)@C-TiO_2) onto a polystyrene substrate; (b) creation of hydrophilic areas (in the closed dash line) by plasma treatment through a mask; (c) revealing the hidden pattern by water exposure.

samples also displayed noticeable color shifts that could be observed easily by the naked eye, with original purple becoming blue and original blue changing to grayish (Fig. 8b,c) in response to ethanol exposure, again with full reversibility. The capability of color change and pattern restoration remained the same after 15 cycles of ethanol addition and evaporation, demonstrating excellent cyclability.

To make the color response more unique, we have combined the three hollow samples to produce a multicolored butterfly pattern, with the body of the butterfly being made of the gray sample, the top wings blue, and the bottom wings purple, as shown in Fig. 9a. All three parts simultaneously displayed a distinct color change when ethanol was sprayed onto the pattern, and then fully reverted to their original colors as the surrounding medium was restored to air upon ethanol evaporation. Similarly, the colors of letters of "UCR" could shift and recover in response to ethanol exposure and evaporation (Fig. 9b). The responsive property of the dual-color pattern was further investigated. Purple and blue colored hollow C-TiO_2 nanoshells were utilized to produce a panda pattern onto a polystyrene substrate (Fig. 9c). When the pattern was soaked in ethanol, the dual-color had a quick switch from purple to deep blue and light blue to gray. As the structural color is caused by Mie resonance and C-TiO_2 is chemically stable, these novel color materials are extremely durable and free from photobleaching. In addition, all the color shifts are distinct, responsive, and reversible, making them potentially useful for applications such as anti-counterfeiting or solvent sensors.

We further designed a solvent-responsive pattern containing hidden information that can only be revealed by exposing the sample to proper solvents. The purple hollow C-TiO_2 nanoshells were first modified with trimethoxy(octadecy)silane to become hydrophobic (see details in the experimental section) and then sprayed onto a polystyrene substrate into a panda pattern, as shown in Fig. 10a. Water beaded up on the film, indicating hydrophobicity (Fig. S7). Then, selected areas in the closed dash line (Fig. 10b) were made hydrophilic by treating with oxygen plasma, which, however, did not lead to any color contrast to the untreated areas. When the panda pattern was placed in water, the hydrophilic sections displayed a notable color change to light blue, while the hydrophobic areas kept the original purple color (Fig. 10c). Thus, the hidden hydrophilic/hydrophobic information was revealed in the form of color pattern with a clear contrast only when the film was exposed to water. Such a unique way of information encryption is believed to find its interesting applications in anti-counterfeiting devices.

Conclusions

We demonstrate in this work the synthesis of C-TiO_2 nanoshells that can display various colors depending on their diameters. While both TiO_2 and carbon are not considered color materials, their unique combination in the form of composite nanoshells enables the striking structural colors of purple, blue and green through the visible resonant Mie scattering: the hollow structure reduces the random multiple scattering and produce the color, and the incorporated carbon species acts as an internal black background to reduce the forward scattering and enhance the color contrast. These two mechanisms work together to make the Mie resonance highly perceptible to the naked eye. Without the need of any external black background, these materials can be conveniently used as alternative pigments, with the intrinsic advantages of structural coloration such as the high optical stability against bleaching, as well as the material-specific beneficial properties such as high chemical stability and low toxicity. Furthermore, the structural color resulting from the visible Mie scattering is highly responsive to the changes in the surrounding medium with full reversibility, making these new materials ideal candidates for a wide range of applications including displays, colorimetric sensors and detectors, and anti-counterfeiting devices.

Conflicts of interest

There are no conflicts to declare.

Acknowledgements

Financial support for this project was provided by the National Natural Science Foundation of China (No. 51702023, 51702022), Natural Science Foundation of the Higher Education Institutions of Jiangsu Province, China (17KJB430001). Yao acknowledges the fellowship support by Nanjing University of Science and Technology. Yin is grateful for the financial support from the U.S. National Science Foundation (DMR-1810485). We also thank Dr. Kerry M. Hanson for help with the measurement of reflectance spectra.

References

1 A.C. Arsenault, D.P. Puzzo, I. Manners, G.A. Ozin, *Nature Photon,* 2007, **1**, 468.
2 M. Wang, L. He, W. Xu, X. Wang, Y. Yin, *Angew. Chem. Int. Ed,* 2015, **54**,7077.
3 W. Lu, H. Ma, F. Mou, M. Zhu, J. Yan, J. Guan, *Adv. Mater,* 2014, **26**, 1058.
4 M.G. Han, C.G. Shin, S.J. Jeon, H.S. Shim, C.J. Heo, H. Jin, J.W. Kim, S.Y. Lee, *Adv. Mater,* 2012, **24**, 6438.
5 J. Ge, Y. Yin, *Angew. Chem. Int. Ed,* 2011, **50**, 1492.
6 G. Mie, *Ann. Phys*, 1908, **25**, 377.
7 M. Retsch, M. Schmelzeisen, H.J. Butt, E.L. Thomas, *Nano Lett,* 2011, **11**, 1389.
8 L.A. Fielding, O.O. Mykhaylyk, A. Schmid, D. Pontoni, S.P. Armes, P.W. Fowler, *Chem. Mater,* 2014, **26**, 1270.
9 Q. Ye, H. Yoshikawa, S. Bandow, K. Awaga, *Appl. Phys. Lett,* 2009, **94**, 063114.
10 P. Zhang, X.W. Lou, *Adv. Mater,* 2019, **31**, 1900281.
11 B. Guan, L. Yu, J. Li, X.W. Lou, *Sci. Adv,* 2016, **2**, e1501554.
12 L. Yu, X. Yu, X.W. Lou, *Adv. Mater,* 2018, **30**, 1800939.

13 J. Hou, H. Zhang, J. Lin, X. Qiu, W. Zhao, X. Sun, Y. Xiang, H. Zhang, G. Xing, D. Zheng, G. Li, Z. Tang, *J. Mater. Chem. A,* 2019, DOI: 10.1039/C9TA02279A.
14 Q. Zhang, X. Jin, Z. Xu, J. Zhang, U.F. Rendón, L. Razzari, M. Chaker, D. Ma, *J. Phys. Chem. Lett,* 2018, **9**, 5317.
15 X. Xie, K. Huang, X. Wu, *J. Mater. Chem. A,* 2018, **6**, 6754.
16 W. Stöber, A. Fink, E. Bohn, *J. Colloid Interface Sci.* 1968, **26**, 62.
17 J.B. Joo, I. Lee, M. Dahl, G.D. Moon, F. Zaera, Y. Yin, *Adv. Funct. Mater,* 2013, **23**, 4246.
18 X. Yang, C. Cao, L. Erickson, K. Hohn, R. Maghirang, K. Klabunde, *J. Catal,* 2008, **260**, 128.
19 Y. Park, W. Kim, H. Park, T. Tachikawa, T. Majima, W. Choi, *Appl. Catal. B* 2009, **91**, 355.
20 M. Xiao, H. Chen, Ti. Ming, L. Shao, J. Wang, *ACS Nano,* 2010, **4**, 6565.
21 H. Xu, X. Chen, S. Ouyang, T. Kako, J. Ye, *J. Phys. Chem. C* 2012, **116**, 3833.
22 X. Yao, C. Zhao, R. He, X. Liu, *Mater. Chem. Phys,* 2013, **141**, 705.
23 F. Tian, Y. Zhang, J. Zhang, C. Pan, *J. Phys. Chem. C* 2012, **116**, 7515.
24 X. Lü, W. Yang, Z. Quan, T. Lin, L. Bai, L. Wang, F. Huang, Y. Zhao, *J. Am. Chem. Soc,* 2014, **136**, 419.
25 L. Sinatra, A.P. LaGrow, W. Peng, A.R. Kirmani, A. Amassian, H. Idriss, O.M. Bakr, *J. Catal,* 2015, **322**, 109.
26 J.D. Forster, H. Noh, S.F. Liew, V. Saranathan, C.F. Schreck, L. Yang, J.G. Park, R.O. Prum, S.G.J. Mochrie, C.S. O'Hern, H. Cao, E.R. Dufresne, *Adv. Mater,* 2010, **22**, 2939.
27 Y. Takeoka, S. Yoshioka, A. Takano, S. Arai, K. Nueangnoraj, H. Nishihara, M. Teshima, Y. Ohtsuka, T. Seki, *Angew. Chem. Int. Ed,* 2013, **52**, 7261.
28 C. Mäetzler, MATLAB functions for Mie scattering and absorption, Version 2, University of Bern, Institute of Applied Physics: Bern, 2002.
29 C.F. Bohren, D.R. Huffman, Absorption and scattering of light by small particles, Wiley, New York 1983.
30 S.M. Scholz, R. Vacassy, J. Dutta, H. Hofmann, *J. Appl. Phys,* 1998, **83**, 7860.
31 K.B. Strawbridge, F.R. Hallett, *Can. J. Phys,* 1992, **70**, 401-406.

